Electron-impact vibrational excitation of furan

L. R. Hargreaves, R. Albaridy, G. Serna, M. C. A. Lopes, and M. A. Khakoo

Phys. Rev. A **84**, 062705 — Published 8 December 2011

DOI: 10.1103/PhysRevA.84.062705

The electron impact vibrational excitation of furan.

L. R. Hargreaves[1], R. Albaridy[1], G. Serna[1], M. C. A. Lopes[2] and M. A. Khakoo[1a].

[1] Department of Physics, California State University, Fullerton, CA 92834, USA.

[2] Departamento de Física, ICE, Universidade Federal de Juiz de Fora, Juiz de Fora-MG, CEP 36036-330, Brazil.

Abstract: We report the first measurements of differential cross-sections for the vibrational excitation of furan (C_4H_4O), obtaining results for nine features spanning the electron energy loss range from 0 to 0.8eV, at electron impact energies of 5, 6, 7.5, 10 and 15eV and for scattering angles ranging from 10^o to 130^o. The normalization of the differential cross-sections was done using elastic differential cross-sections for furan determined earlier by our group (Khakoo *et al.*, Phys. Rev A. **81**, 062716, 2010).

Pacs #s: 34.80.Dp, 34.80.Gs, 34.80.Ht

[a] Author to whom correspondence should be addressed. Electronic mail: mkhakoo@fullerton.edu

1. Introduction.

Much recent activity in the study of low energy electrons interacting with polyatomic targets has been instigated by the important work of Sanche and co-workers [1], who experimentally demonstrated that single- and double-strand breaks in DNA are induced by secondary low-energy electrons (below 20eV), which therefore can contribute to the damaging effects of ionizing radiation on living cells and tissues. This discovery has especially stimulated studies in biologically relevant molecules that aim to provide insights into mechanisms for radiation damage of DNA by slow electrons, including both direct processes such as ionization and electronic or vibrational excitation and processes involving compound states or resonances, notably dissociative electron attachment. Many of these studies involve structural units of DNA, such as the phosphate group, the deoxyribose sugar or the nucleobases [2–4], or else involve molecules structurally or functionally similar to such DNA subunits [3,5–9]. We note a recent investigation of the effect of neighboring water on the location of π^* shape resonance in formaldehyde [10] as a step toward understanding solvation effects in DNA-related molecules. A particular feature that many of these molecules have in common is the presence of a first excited triplet state lying at around 3 to 4 eV [11] above the ground state. Relevant within this context, and also well recognized, is the fact that at this range of electron impact energies, the inclusion of polarization effects is very important for an accurate description of the scattering process, especially with regard to the determination of the resonances' positions. Taking the above considerations in mind, we chose furan (C_4H_4O) because it represents a simpler but similar system to the tetrahydrofuran molecule (C_4H_8O), a model of the sugar component of the backbone of the DNA, and also because it presents two prominent shape resonances around the $^3B_2$ excitation threshold [12–14]. Theoretical calculations on electron collisions with furan were recently performed by Bettega and Lima

[9], by da Costa *et al.* [15] and by Khakoo *et al.* [16]. These calculations revealed the importance of polarization effects in the description of elastic as well as electronically inelastic processes and produced elastic cross-sections for furan in very good agreement with experiment [16]. A closely related molecule, tetrahydrofuran (THF), has been studied in the gas phase by several groups [5,8,17-19], the most recent study being that of Allan [19]. Different theoretical methods and approaches also addressed elastic and inelastic electron scattering by THF [2,3,7,20,21]. Although both molecules are quite similar from a structural standpoint, it should be noted that tetrahydrofuran has a much larger dipole moment (1.75D) [22] than furan (0.67D) [23].

Initial angle-differential energy loss (E_L) spectroscopic studies of furan were done at an incident energy (E_0) of 50eV by Flicker *et al*. [24,25] who obtained relative differential cross-sections (DCS) for scattering angles (θ) up to 80^o for excitation to the low-lying triplet $^3B_2$ and $^3A_1$ states of furan, thiophene (C_4H_4S) and pyrrole (C_4H_4NH), the latter two being similar cyclic compounds. A high-resolution study of the vibrational structure overlaying these two triplet bands of furan was done by Giuliani *et al.* [26] at an E_0 of 30eV and θ values of 10^o and 25^o. A similar recent study by Motte-Tollet *et al.* [27], from the same laboratory as [26], focused on the vibrational excitation of furan at a fixed scattering angle of 30^o for incident energies (E_0) from 3 to 10eV. They identified energy loss structures belonging to the vibrational bands observed by Rico *et al.* [28], Scott [29,30] and Klots *et al.* [31] using Raman and infra-red (IR) absorption spectroscopy (in both gas and liquid phase). Assignments of the normal modes were made by Rico *et al.* [28] and Orza *et al.* [32] using semi-empirical force-constants applied to the various bands observed in furan and its deuterated derivatives. Scott [29,30] revisited the results of [28,32] and assigned the character of vibrational modes using a global least-squares constraint on the furan force field to fit observed modes simultaneously.

Scott [30] also illustrated the vibrational modes of furan, which were subsequently investigated further by Klots *et al.* [31], who measured the Raman and IR spectrum of furan and refined the earlier assignment of vibrational modes. A more recent and extensive study of the vibrational infra-red spectrum of furan was reported by Mellouki *et al.* [33], who measured a high resolution, Fourier transform IR spectrum of furan over a broad spectral range, using modern computational software (Gaussian™ [34] at the MP2 level) to compute normal mode coordinates and thus updated the assignments of the vibrational modes. Computed bond angles and vibrational mode band intensities, as well as detailed three-dimensional drawings of these modes, are given in their paper, to which we will mostly refer to here.

Recently, total cross-sections for electron scattering from furan molecules were determined for E_0 from 0.6eV to 400eV using a linear electron-transmission method by Szmytkowski *et al.* [35]. They observed resonance structures at E_0=1.8eV and 3.1eV, consistent with the work of Modelli and Burrow [12], followed by another maximum around E_0=8eV in very good agreement with [12] and also with recent calculations by Bettega and Lima [9] and by Khakoo *et al*. [16].

The present work reports DCSs for vibrational excitation features in electron energy loss spectra of furan in the E_L range of 0 to 0.8eV, taken at E_0 values of 5.0, 6.0, 7.5, 9.0, 10.0 and 15.0eV and for θ in the range of 10^o to 130^o. The DCSs were obtained by normalizing the spectral intensities to our earlier elastic electron scattering DCS measurements [16].

A solid molecular model of furan is shown in figure 1. It is a planar molecule in its ground electronic state and belongs to the C_{2v} symmetry group. It has a twofold axis of rotation which contains the oxygen atom and also two vertical planes of symmetry, leading to four symmetry species, A_1, A_2, B_1, B_2 (see [36]), which represent 21 normal vibrational modes. The direct product table for this symmetry is given in table 1 [36] and the character table can be obtained

from references 33 and 36. Table 2 shows a summary of the pertinent vibrational modes of furan covered in this work, including IR intensities of the various bands based on the intensities given in [33] and [28] as well as the energies of the individual normal modes. Detailed illustrations of the vibrational modes of furan are given by [33] and earlier by [31]. In this work we will use the labeling of modes given by Mellouki *et al*. [33], who reverse the labeling of B_1 and B_2 compared to earlier work.

2. Experimental.

The experimental apparatus has been described in previous articles, e.g. Khakoo *et al.* [37], so only a brief description will be given here. The electron gun and the detector employed double hemispherical energy selectors which were made of titanium. Cylindrical (titanium) lenses equipped with molybdenum apertures were used to transport, focus and collimate electrons emitted from a thoriated tungsten cathode, and the system was baked to about 130°C with magnetically free biaxial heaters (ARi Industries model BXX06B41-4K). The analyzer's detector was a discrete dynode electron multiplier (Equipe Thermodynamique et Plasmas model AF151) with a background rate of <0.01 Hz and the capability of linearly detecting electron count rates of up to 1MHz of electrons without saturating. The remnant magnetic field in the collision region was reduced to less than 1 mG by using a double μ-metal shield as well as a coil that reduced the vertical component of the Earth's magnetic field. Typical electron currents at the collision region were around 30 nA, with an energy resolution of 70 meV, full width at half maximum. The larger current is more desirable for shorter spectrum acquisition periods. The electron beam remained stable to within 20% over a period of several days, requiring minor tuning of the spectrometer to maintain the long-term stability of the current to within 5%. The energy of the beam was established by determining the cut-off in the energy

loss spectrum at zero residual energy, which was found to be in agreement with the dip in the He elastic-scattering cross section due to the $2\,^2S$ He^- resonance at 19.366 eV [38]. Typically the contact potential, so determined, stayed between 0.8 to 0.9 eV, with an uncertainty of 40meV, over the multi-week course of the experiments. Energy-loss spectra of the elastic peak were collected at fixed E_0 values and θ by repetitive multichannel-scaling techniques. The angular resolution was 2°, full width at half maximum. The effusive target gas beam was formed by flowing gas through a thin aperture source 0.3mm in diameter described previously [39]. This source was covered with carbon soot, using a pure acetylene flame, to reduce secondary electrons and placed 6 mm below the axis of the electron beam, incorporated into a movable source arrangement [40]. The movable gas source method determines background scattering rates expediently and accurately. The vapor pressure behind the source for furan was about 0.3 to 0.4 Torr the pressure in the experimental chamber ~4×10^{-6} Torr. The gas beam temperature, determined by the apparatus temperature in the collision region, was about 130°C; however, in most of the gas handling copper tubing, the temperature was 24°C. The higher temperature was in the last 4 cm of the gas handling system before the gas exited into the collision region. Furan vapor was obtained from stabilized liquid furan (>99.0% purity) which was degassed using freeze-pump-thaw cycles.

4. Results and discussion.

A section of the energy-loss spectrum below 1eV is shown in figure 2. As seen in to this spectrum, the resolution of the present spectrometer (see above) was not sufficient to separate all the vibrational features. Similar to [27], we were able to identify seven features located at the E_L values of 0.092, 0.128, 0.178, 0.214, 0.269, 0.391, 0.514eV energy loss, as well as two further features at 0.580 and 0.767eV energy loss, which were not covered by

[27]. These features are indicated by arrows in figure 2. Of them, only the E_L=0.269eV feature is an isolated excitation, being a B_2 symmetry $\nu_7+\nu_{19}$ combination band involving two C-H in-plane bending vibrations [33] (table 2). The rest of the observed features are the sum of several vibrational modes, as given in table 2 from the spectroscopic work of [33]. These were unfolded in the conventional way, using the elastic feature as representative of the spectrometer's line profile. An example of this unfolding is shown in figure 2. No correction for the spectrometer transmission was made because the E_0 of this work was much greater than the E_L measured in the vibrational spectrum. Our smallest E_0 was 6.6 times the largest E_L measured, while we would expect our spectrometer's characteristic transmission factors to deviate from unity by >0.10 only for E_0/E_L ratios around ≈3 or less. In the present work, the energy resolution of the spectrometer was insufficient to readily separate the E_L = 0.092eV feature from the elastic peak, and consequently the uncertainties in the measured cross sections this feature are significantly enlarged. In some cases the 0.092eV feature was too weak to extricate from the elastic and its intensity was marked to zero. From figure 2 it can be seen that the E_L=0.391eV feature is a dominant part of the vibrational energy loss spectrum. This is made up of the four CH stretching normal modes that arise from different linear combinations of the individual C-H stretches, i.e. two A_1 and two B_2 modes; these are observed as medium or shoulder features in IR spectroscopy, as indicated in table 2, but are readily seen in the electron energy loss spectrum as a combined feature.

Our DCSs are plotted in figures 3. We have only selected a portion of our DCSs in this figure (at E_0=5eV, 7.5eV and 15eV) to save space. The full set is shown in table 3, with average error bars. Complete point-by-point error tables of our data may be obtained from [41]. From table 1, it can be seen that all excitations from the ground A_1 symmetry state except those with A_2 symmetry are dipole-allowed, since each of the A_1, B_1 and B_2 representations contains

component of the electric dipole operator D_i (see table 2). One might therefore expect all excitations listed in table 2 to show the forward-peaked DCS characteristic of dipole-allowed transitions. However, we observe from figures 3a-c, that this is not at all the case. In fact, the only forward-peaked DCSs are those of the E_L = 0.092eV, 0.128eV, 0.178eV and 0.214eV features. The dipole-allowed E_L=0.391eV feature (CH stretch modes) which is a dominant feature in the energy loss spectra does not show forward scattering at all E_0 values. The overall picture seems to be somewhat consistent, however, with table 2. The energy-loss features containing modes with large dipole transition-moments ("strong" or "very strong" in the IR spectrum) show some forward scattering, whereas the CH stretch modes are "not observed" to at most "medium" in the IR spectrum. At either E_0=5eV or 15eV (or both) these features show forward peaking, despite the limitation of these measurements which do not go below $\theta=10^o$, where likely these features will show even more strongly pronounced forward-peaking. Nevertheless, the E_L=0.092eV feature does display dipole behavior, as shown in the figures 3a-c at low energies. At 15eV, this feature shows a rise at $\theta=10^o$, but our measurements do not extend below this angle. Data at higher energy resolution and smaller θ are required to establish this trend on a firmer basis to see if indeed the forward-scattering is visible at extremely low θ.

Figure 3d shows the DCSs for excitation of the E_L=0.269eV feature which is the only single vibrational mode feature, i.e. a B_2 symmetry $\nu_7 + \nu_{19}$ combination mode (both in-plane CH bending vibrations). This feature shows a characteristic weak and non-dipole behavior as is observed in IR-spectroscopy, showing a mostly flat angular distribution similar to that of the other features with low dipole transition-moments, which display a flat behavior (E_L=0.391, 0.580 and 0.767eV features) or a slight backward scattering profile (in the case of the 0.514eV feature) at E_0=5eV and 7.5eV, developing into a peak at scattering angles around 40-60^o at

E_0=15eV. We note here that the two strong features that are easily discerned from the spectrum are those at E_L values of 0.128eV (dipole favored component) and 0.391eV (CH stretch modes, with a medium-to-weak transition moment in the dipole, but strongly excited via electric quadrupole; this combined feature is very strong in the Raman spectrum – see table 2)., i.e. two energy loss features with different angular behavior. Lastly, figure 3e shows the DCSs for the sum of all the vibrational modes. If one excludes the lowest θ point, it is evident that forward scattering is minimal. Certainly this forward-scattering, if any, is much weaker than what has been observed in other molecules, e.g. in the vibrational excitation of H_2O (see e.g. [42])

The DCSs for electron impact vibrational excitation were visually extrapolated to $\theta=0^o$ and $\theta=180^o$, and then solid-angle integrated to yield electron impact vibrational excitation integral cross-sections (ICS). To estimate the uncertainty in extrapolation, we also "flat-extrapolated" these DCSs, and the difference between the visual and flat extrapolations was added, in quadrature, to the average DCS error to form the error on the ICS obtained. Figure 4a-c shows these ICSs for the nine E_L features which are listed in table 4, and figure 4d shows the summed ICSs for all the vibrational transitions. We note that the ICSs of all these features peak in the E_0 range of these measurements. The most intense feature at E_L=0.128eV is found to peak at $E_0\approx$7.5eV as do several other features, viz. those at E_L=0.178eV, 0.269eV, 0.391eV, 0.580eV and 0.751eV. The summed ICSs in figure 4d show a clear maximum around $E_0\approx$8eV. Core-excited Feschbach resonances for furan occur between 3.5 and 10.7 eV [43], with a large maximum around 5.55eV, suggesting that those resonances may play a role in vibrational excitation of furan. Indeed, the dissociative attachment studies of Sulzer et al. [13] show a resonant production of negative ions centered around 6eV, adding to the picture but not completely explaining our results, in which the maximum occurs at 8eV. The higher-energy

maximum in the vibrational ICS suggests that direct (nonresonant) excitation and possibly one or more high-lying shape resonances are also important mechanisms which could populate the vibrational states through electron impact.

The feature at E_L=0.092eV peaks at a much higher E_0 of around 12eV, whereas the E_L=0.514eV feature peaks between 6eV and 7.5eV, indicating that only the second feature at E_L=0.128eV may be related to processes which lead to the resonant furan dissociation. The E_L=0.214eV feature appears to show an abnormal behavior, which we attribute to its position being sandwiched in between other more dominant features, i.e. E_L=0.178eV and the 0.269eV features. The error bars of this feature are the largest of all the features.

Missing, of course, in all of the IR spectra is the excitation of A_2 symmetry vibration modes, i.e. ν_9, ν_{10} and ν_{11} in [33] which are out-of-plane vibrations involving either CH bending or ring deformations. Whereas these cannot be excited by photons, they should be readily accessible to excitation by electrons; thus, these modes, which lie at E_L=0.076eV, 0.090eV and 0.108eV, could be important components of the E_L=0.092eV feature and should be included in computational models of electron scattering by furan. For such forbidden-symmetry IR transitions, it would be valuable to extend these measurements to lower E_0 values in a similar way as was done by [26] to look at the vibrational excitation of the low lying triplet states of furan.

5. Conclusions.

We present the first measurements of differential cross-sections for the vibrational excitation of furan by low-energy electron impact. The results show that the DCSs behave consistently with the nature of the transition moments of the excited vibrational modes comprising the features measured, as observed in IR and Raman spectroscopy and summarized

in table 2 for this work. However, the forward scattering expected for dipole-allowed excitations is in most cases is not observed. We have extended the study of Motte-Tollet *et al.* [27] by including two additional features, at E_L=0.580eV and 0.767eV, which are weak but clearly observed in our energy loss spectra. Since the measurements were not able to resolve most individual vibrational modes, this work should be viewed as a pilot study which needs to be superseded by higher resolution measurements at lower E_0 values, with an aim to investigate more closely the forward scattering vibrational modes making up the E_L=0.092eV, 0.129eV, 0.178eV and 0.218eV features and to investigate the dominant CH stretch ν_1 mode at E_L=0.393eV. Calculations of vibrational excitation cross sections that could shed light on the collision dynamics would also be quite useful.

6. Acknowledgements

This work was sponsored by the US National Science Foundation under Grants PHY 0653452 research in an undergraduate institution. M. C. A. L. would like to acknowledge the financial support from the Brazilian agency Conselho Nacional de Desenvolvimento Cientíifico e Tecnológico (CNPq) and Fundação de Amparo à Pesquisa do Estado de Minas Gerais (FAPEMIG). This work is part of a collaborative project involving funding from NSF (above) and CNPq (Project No. 490415/2007–5). M. A. K. thanks Dr. Carl Winstead (California Institute of Technology, Pasadena, CA, USA) for useful comments and discussions regarding this manuscript.

7. References.

[1] B. Boudaïffa, P. Cloutier, D. Hunting, M. A. Huels, and L. Sanche, Science **287**, 1658 (2000); L. Sanche, Eur. Phys. J. D **35**, 367 (2005); F. Martin, P. D. Burrow, Z. Cai, P. Cloutier, D. Hunting, and L. Sanche, Phys. Rev. Lett. **93**, 068101 (2004).

[2] P. Mozejko and L. Sanche, Radiat. Phys. Chem. **73**, 77 (2005).

[3] C. Winstead and V. McKoy, J. Chem. Phys. **125**, 244302 (2006).

[4] C. Winstead and V. McKoy, J. Chem. Phys. **125**, 074302 (2006).

[5] A. Zecca, C. Perazzolli, and M. J. Brunger, J. Phys. B **38**, 2079 (2005).

[6] C. König, J. Kopyra, I. Bald, and E. Illenberger, Phys. Rev. Lett. **97**, 018105 (2006).

[7] C. S. Trevisan, A. E. Orel, and T. N. Rescigno, J. Phys. B **39**, L255 (2006).

[8] C. J. Colyer, V. Vizcaino, J. P. Sullivan, M. J. Brunger, and S. J. Buckman, New J. Phys. **9**, 41 (2007).

[9] M. H. F. Bettega and M. A. P. Lima, J. Chem. Phys. **126**, 194317 (2007).

[10] T. C. Freitas, M. A. P. Lima, S. Canuto and M. H. F. Bettega, Phys. Rev. A **80**, 062710 (2009).

[11] T. Fleig, S. Knecht, and C. Hättig, J. Phys. Chem. A **111**, 5482 (2007).

[12] A. Modelli and P. W. Burrow, J. Phys. Chem. A **108**, 5721 (2004).

[13] P. Sulzer, S. Ptasinska, F. Zappa, B. Mielewska, A. R. Milosavljevic, P. Scheier, T. D. Märk, I. Bald, S. Gohlke, M. A. Huels, and E. Illenberger, J. Chem. Phys. **125**, 044304 (2006).

[14] M. H. Palmer, I. C. Walker, C. C. Ballard, and M. F. Guest, Chem. Phys. **192**, 111 (1995).

[15] R. F. da Costa, M. H. F. Bettega and M. A. P. Lima, Phys. Rev. A **77**, 012717 (2008).

[16] M. A. Khakoo, J. Muse, K. Ralphs, R. F. da Costa, M. H. F. Bettega and M. A. P. Lima, Phys. Rev A. **81**, 062716 (2010).

[17] B. C. Ibanescu, O. May and M. Allan, Phys. Chem. Chem. Phys. **10**, 1507 (2008).

[18] A. Aflatooni, A. M. Scheer and P. D. Burrow, J. Chem. Phys. **125**, 054301 (2006).

[19] M. Allan, J. Phys. B **40**, 3531 (2007).

[20] S. Tonzani and C. H. Greene, J. Chem. Phys. **125**, 094504 (2006).

[21] F. Blanco and G. Garcia, Phys. Lett. A **360**, 707 (2007).

[22] *CRC Handbook of Chemistry and Physics,* 90th ed., D. R. Lide and W. M. Haynes, eds. (CRC Press, Boca Raton, 2009), p. 9-58.

[23] Jung Jin Oh, Kurt W. Hillig II, Robert L. Kuczkowski, J. Phys. Chem. **94**, 4453 (1990).

[24] W. M. Flicker, Orkti A. Mosher and Aron Kuppermann, Chem. Phys. Letts., **38**, 489 (1976).

[25] W. M. Flicker, Orkti A. Mosher and Aron Kuppermann, J. Chem. Phys., **64**, 1315 (1976).

[26] A. Giuliani, M.-J. Hubin-Franskin, Int. J. Mass Spectroscopy, **205**, 163 (2001).

[27] F. Motte-Tollet, G. Eustatiu and D. Roy, J. Chem. Phys., **7448**, 1315 (1996).

[28] M. Rico, M. Barrachina and J. M. Orza, J. Molec. Spectroscopy, **24**, 133 (1967).

[29] D. W. Scott, J. Molec. Spectroscopy, 31, 77 (1969).

[30] D. W. Scott, J. Molec. Spectroscopy, **37**, 77 (1971).

[31] T. D. Klots, R. D. Chirico and W. V. Steele, Spectrochim. Acta, **50A**, 765 (1994).

[32] J. M. Orza, M. Rico and M. Barrachina, J. Molec. Spectroscopy, **20**, 233 (1966).

[33] A. Mellouki, J. Léivin and M. Herman, Chem. Phys., **271**, 239 (2001).

[34] M. Frisch *et al.*., Gaussian, Inc., Pittsburgh, PA (1998).

[35] C. Szmytkowski, P. Możejko, Eliżabieta Ptasińka-Denga and Agnieska Sabisz, Phys. Rev. A **82**, 032701 (2010).

[36] J. I. Steinfeld, *Molecules and Radiation: An Introduction to Modern Molecular Spectroscopy*, The MIT Press Cambridge, Massachusetts and London, England, Edition 4 (1984).

[37] M. A. Khakoo, C. E. Beckmann, S. Trajmar, and G. Csanak, J. Phys. B **27**, 3159 (1994).

[38] J. H. Brunt, G. C. King, and F. H. Read, J. Phys. B **10**, 1289 (1977).

[39] M. A. Khakoo, H. Silva, J. Muse, M. C. A. Lopes, C.Winstead, and V. McKoy, Phys. Rev. A **78**, 052710 (2008).

[40] M. Hughes, K. E. James Jr., J. G. Childers, and M. A. Khakoo, Meas. Sci. Technol. **14**, 841 (1994).

[41] mkhakoo@fullerton.edu

[42] M. A. Khakoo, C. Winstead, V. McKoy, Phys. Rev. A **79**, 057211 (2009).

[43] M. V. Muftakhov, N. L. Asfandiarov, and V. I. Khvostenko, J. Electron Spectrosc. Relat. Phenom. **69**, 165 (1994).

Table and Table Captions.

C_{2V}	A_1	A_2	B_1	B_2	Transition Operators
A_1	A_1	A_2	B_1	B_2	$D_z, D^2_{xx}, D^2_{yy}, D^2_{zz}, \alpha_{xx}, \alpha_{yy}, \alpha_{xx}$
A_2	A_2	A_1	B_2	B_1	R_z, D_{xy}, α_{xy}
B_1	B_1	B_2	A_1	A_2	$D_x, R_y, D^2_{xz}, \alpha_{xz}$
B_2	B_2	B_1	A_2	A_1	$D_y, R_x, D_{yz}, \alpha_{yz}$

Table 1: Direct product tables and transition-moment operator symmetries for a molecule with C_{2V} symmetry (from Steinfeld, [33]). The non-zero transition operators connecting these direct products are also given. D_i are the components of the dipole operator along the respective axes in figure 1. D_{ij} are the electric quadrupole operators, which are also related to their derivative Raman operators, $\alpha_{ij,}$. R_i are the magnetic dipole operators. See text.

E_L												
		[33]		[33]			[31] [32]		[27] [33]	[32],[33] Intensity	
Present	[27]	eV	1/cm	Symmetry	I.D.	A_i (kJ/mole)	Symmetry	I.D.	Mode	I.R.	Raman
0.092	0.093	0.0747	602.85	B_1	ν_{14}	18.90	B_2	ν_{21}	γ_{ring}	S	W
		0.0923	744.65	B_1	ν_{13}	106.60	B_2	ν_{20}	γ_{CH}	VS	VW
		0.1038	837.59	B_1	ν_{12}	0.02	B_2	ν_{19}	γ_{CH}	VW	W
0.128	0.129	0.1233	994.68	A_1	ν_7	37.80	A_1	ν_7	δ_{CH}	VS	M
		0.1293	1042.5	B_2	ν_{20}	0.01	B_1	ν_{17}	δ_{ring}	NO	M
		0.1323	1067.22	A_1	ν_6	9.70	A_1	ν_6	δ_{CH}	S	M
		0.1414	1140.2	A_1	ν_5	0.03	A_1	ν_5	ν_{ring}	NO	VS
		0.1464	1180.97	B_2	ν_{19}	25.70	B_1	ν_{16}	δ_{CH}	VS	W
0.178	0.179	0.1717	1384.5	A_1	ν_4	5.50	A_1	ν_4	ν_{ring}	M	S
		0.1848	1490.55	A_1	ν_3	16.30	A_1	ν_3	ν_{ring}	S	VS
		0.1931	1557.5	B_2	ν_{17}	0.01	B_1	ν_{14}	ν_{ring}	W	VW
0.214	0.218	0.1959	1580.37	A_1	$\nu_{12}+\nu_{13}$	< 1.80	A_1	$\nu_{19}+\nu_{20}$	$\gamma_{CH}+\gamma_{CH}$	M	-
		0.2106	1698.82	B_2	$\nu_9+\nu_{12}$	< 0.02	B_1	$\nu_9+\nu_{19}$	$\gamma_{CH}+\gamma_{CH}$	W	-
		0.2140	1726.28	B_2	$\nu_8+\nu_{21}$	< 0.01	B_1	$\nu_8+\nu_{18}$	$\delta_{ring}+\delta_{ring}$	VW	-
		0.2189	1765.8	B_1	$\nu_{11}+\nu_{19}$	< 0.01	B_2	$\nu_{11}+\nu_{16}$	$\gamma_{ring}+\delta_{CH}$	VW	-
		0.2272	1832.58	B_1	$\nu_7+\nu_{12}$	< 0.01	B_2	$\nu_7+\nu_{19}$	$\delta_{CH}+\gamma_{CH}$	VW	-
0.269	0.269	0.2692	2171.5	B_2	$\nu_7+\nu_{19}$	< 0.02	B_1	$\nu_7+\nu_{16}$	$\delta_{CH}+\delta_{CH}$	W	VW(liq)
0.391	0.392	0.3881	3130.15	B_2	ν_{16}	1.20	B_1	ν_{13}	ν_{CH}	M	S
		0.3893	3139.84	A_1	ν_2	< 0.03	A_1	ν_2	ν_{CH}	OV	OV
		0.3919	3160.75	B_2	ν_{15}	0.17	B_1	ν_{12}	ν_{CH}	M	M
		0.3930	3169.4	A_1	ν_1	0.01	A_1	ν_1	ν_{CH}	NO	VS
0.514	0.514	0.5149	4152.75	A_1	$\nu_{16}+\nu_{20}$	< 1.2	A_1	$\nu_{13}+\nu_{17}$	$\nu_{CH}+\delta_{ring}$	M	-
		0.5180	4177.58	B_2	$\nu_6+\nu_{16}$	< 1.2	B_1	$\nu_6+\nu_{13}$	$\delta_{CH}+\nu_{CH}$	M	VW
		0.5207	4199.45	A_1	$\nu_{15}+\nu_{20}$	< 0.17	A_1	$\nu_{12}+\nu_{17}$	$\nu_{CH}+\delta_{ring}$	M	VW
0.580		0.5600	4516.76	B_2	$\nu_4+\nu_{16}$	< 0.01	B_1	$\nu_4+\nu_{13}$	$\nu_{ring}+\nu_{CH}$	VW	-
		0.5631	4541.27	B_2	$\nu_4+\nu_{15}$	< 0.01	B_1	$\nu_4+\nu_{12}$	$\nu_{ring}+\nu_{CH}$	VW	-
		0.5640	4548.85	A_1	$\nu_1+\nu_4$	< 0.01	A_1	$\nu_1+\nu_4$	$\nu_{CH}+\nu_{ring}$	VW	-
		0.5725	4617.7	B_2	$\nu_3+\nu_{16}$	< 0.01	B_1	$\nu_3+\nu_{13}$	$\nu_{ring}+\nu_{CH}$	VW	-
		0.5768	4652.43	B_2	$\nu_3+\nu_{15}$	< 0.01	B_1	$\nu_3+\nu_{12}$	$\nu_{ring}+\nu_{CH}$	VW	-
		0.5828	4700.71	B_2	$\nu_2+\nu_{17}$	< 0.01	B_1	$\nu_2+\nu_{14}$	$\nu_{CH}+\nu_{ring}$	VW	-
0.767		0.7628	6151.97	A_1	$2\nu_{CH}$	< 0.02	A_1	$2\nu_{CH}$	$2\nu_{CH}$	W	VW
		0.7649	6169.24	B_2	$2\nu_{CH}$	< 0.02	B_1	$2\nu_{CH}$	$2\nu_{CH}$	W	VW
		0.7665	6182.56	A_1	$2\nu_{CH}$	< 0.02	A_1	$2\nu_{CH}$	$2\nu_{CH}$	W	VW
		0.7710	6218.66	A_1	$2\nu_{CH}$	< 0.02	A_1	$2\nu_{CH}$	$2\nu_{CH}$	W	VW
		0.7750	6250.56	A_1	$2\nu_{CH}$	< 0.02	A_1	$2\nu_{CH}$	$2\nu_{CH}$	W	VW
		0.7775	6271.18	A_1	$2\nu_{CH}$	< 0.02	A_1	$2\nu_{CH}$	$2\nu_{CH}$	W	-

Table 2: Energy loss feature's envelopes observed in this work, considering the dominant vibrational modes of furan, their symmetry (see table 1) and mode nature; ν=stretching vibration; δ= bending vibration; γ= bending out-of-plane vibration. ν_{CH}, refers to the stretch mode of one of the C-H bonds. Spectral data and intensity values are taken from Motte-Tollet *et al.,* [27], Rico *et al.* [28], Klots *et al.* [31] and Mellouki *et al.* [33]. Intensities:- VS: very strong, S: strong, M: medium, W: weak, VW: very weak, NO: not observed, OV: overlapped by another feature. The energy loss E_L (=transition energy) identifies the vibrational excitation feature. The band intensity values A_i are obtained from table 5 of [33] where, from a combination of Rico *et al.* [29] and [33], we estimated the band intensities for mixed-mode band by taking into consideration that the intensity will be less than that of the least intense mode. For illustrations of the vibrational modes see [33] and [31].

E_0=5eV

E_L(eV)→ θ(deg)↓	0.092	0.128	0.178	0.214	0.269	0.391	0.514	0.58	0.751
	DCS								
20	8.72	10.3	3.95	0.894	1.21	8.89	0.656	0.358	0.579
25	2.83	11.0	3.58	0.998	1.44	9.88	0.753	0.416	0.649
30	1.26	5.75	2.50	0.996	1.16	8.69	0.736	0.376	0.542
35	1.12	8.76	2.33	0.677	1.04	7.93	0.712	0.365	0.498
40	0.730	8.20	2.54	0.602	1.13	8.05	0.638	0.423	0.554
50	0	8.59	2.40	0.592	1.22	7.56	0.713	0.480	0.503
60	0.575	8.11	2.10	0.613	1.11	7.60	0.704	0.392	0.465
80	1.33	9.11	2.41	0.596	1.26	7.85	0.972	0.432	0.533
90	2.09	8.62	3.06	0.274	1.36	7.25	1.06	0.402	0.638
105	2.15	8.00	2.87	0.529	1.16	6.07	0.974	0.336	0.514
120	1.97	7.32	2.74	0.338	1.29	5.52	1.04	0.432	0.570
130	2.65	6.96	2.78	0.514	1.17	5.50	1.05	0.372	0.574
Error %	19.7	15.1	15.5	19.6	15.4	15.0	15.5	16.1	15.7

E_0=6eV

E_L(eV)→ θ(deg)↓	0.092	0.128	0.178	0.214	0.269	0.391	0.514	0.58	0.751
	DCS								
15	7.36	11.0	4.33	1.43	1.67	6.69	0.670	0.342	0.591
20	1.69	10.0	1.97	0.571	1.52	6.86	1.439	0.340	0.534
25	1.58	10.2	4.66	0.452	1.93	8.71	0.817	0.523	0.764
30	1.24	9.37	4.40	0.312	1.94	7.94	0.829	0.441	0.559
35	0	9.05	3.80	0.867	1.57	7.89	0.813	0.518	0.612
40	0	9.58	3.25	0.374	1.84	5.67	1.786	0.428	0.572
50	0	9.29	3.62	0.261	1.84	7.80	0.930	0.352	0.593
60	1.17	9.39	3.40	0.352	2.07	7.58	0.879	0.384	0.568
80	0.75	9.15	3.69	0.489	2.30	9.78	1.18	0.582	0.837
90	2.51	11.6	3.68	0.463	2.17	8.58	1.40	0.568	0.649
105	2.38	11.1	3.78	0.384	2.21	7.09	1.26	0.523	0.737
120	0	11.3	3.86	0.363	2.11	7.00	1.14	0.580	0.822
130	0	10.6	4.22	0.652	2.17	7.21	1.40	0.589	0.823
Error %	21.1	15.0	15.2	22.3	15.1	15.0	15.2	15.6	15.3

E_0=7.5eV

E_L(eV)→ θ(deg)↓	0.092	0.128	0.178	0.214	0.269	0.391	0.514	0.58	0.751
	DCS								
10	19.1	14.8	9.68	0.549	2.97	6.63	0.921	0.489	0.681
15	6.51	9.86	6.89	0.37	2.33	6.18	0.863	0.418	0.599
20	8.91	9.14	6.93	0.503	2.43	6.97	0.871	0.488	0.689
25	3.03	8.91	6.57	0.475	2.48	6.83	0.924	0.429	0.549
30	3.31	7.77	6.12	0.404	2.34	6.66	0.837	0.485	0.660
35	1.00	9.68	5.83	0.515	2.44	7.15	0.937	0.516	0.628
40	1.59	10.6	5.96	0.469	2.51	7.57	0.988	0.488	0.686
50	1.89	11.1	5.59	0.433	2.64	7.49	1.07	0.508	0.642
60	1.40	11.1	5.03	0.261	2.54	7.02	1.04	0.452	0.620
80	2.98	15.0	6.41	0.089	3.77	9.48	1.51	0.413	0.815
90	2.88	16.1	6.85	0.336	3.83	9.98	1.53	0.641	0.754
105	2.88	15.2	6.49	0.145	3.51	9.19	1.45	0.758	0.850
120	1.56	14.3	5.84	0.292	3.28	8.26	1.43	0.573	0.774
130	1.80	13.6	6.56	0.062	3.19	8.42	1.37	0.664	0.885
Error %	16.2	14.5	15.1	41.9	14.6	15.0	15.4	16.1	15.6

E_0=10eV

E_L(eV)→ θ(deg)↓	0.092	0.128	0.178	0.214	0.269	0.391	0.514	0.58	0.751
	DCS								
10	26.3	8.58	7.57	0.598	1.64	4.05	0.496	0.179	0.501
20	11.06	3.67	5.03	0.207	1.44	4.12	0.381	0.176	0.481
30	7.40	4.56	4.81	0.381	1.46	4.54	0.501	0.234	0.494
40	5.99	6.05	4.94	0.292	1.66	4.96	0.524	0.298	0.508
50	5.09	8.23	4.98	0.426	1.87	5.65	0.603	0.259	0.692
60	3.29	10.43	5.01	0.387	1.97	5.75	0.775	0.273	0.534
80	3.23	8.28	3.98	0.269	1.55	5.01	0.604	0.215	0.352
90	3.66	8.06	3.85	0.205	1.56	4.80	0.644	0.228	0.333
105	5.49	7.97	3.74	0.307	1.46	5.24	0.589	0.230	0.319
120	6.01	7.98	4.46	0.269	1.65	5.83	0.76	0.228	0.400
130	6.47	8.74	4.05	0.537	1.52	6.43	0.81	0.306	0.547
Error %	15.3	15.1	15.1	24.5	15.2	15.0	15.8	17.9	15.6

E_0=15eV

E_L(eV)→ θ(deg)↓	0.092	0.128	0.178	0.214	0.269	0.391	0.514	0.58	0.751
	DCS								
10	2.69	12.1	1.96	0.967	0.762	1.72	0.195	0.082	0.142
15	0	8.32	2.04	0.72	0.88	1.65	0.195	0.150	0.161
20	0	6.59	2.07	0.557	1.79	1.73	0.158	0.071	0.122
25	1.26	5.42	2.07	0.515	0.783	1.57	0.191	0.056	0.107
30	2.47	5.38	2.79	0.449	0.933	2.04	0.187	0.095	0.166
35	3.17	5.78	2.95	0.663	0.976	2.30	0.261	0.089	0.195
40	2.11	5.50	2.55	0.478	1.01	1.95	0.213	0.109	0.157
50	3.82	6.00	3.33	0.365	1.17	1.95	0.302	0.091	0.206
60	4.55	5.06	3.40	0.276	1.16	1.77	0.280	0.093	0.163
70	0	5.81	2.04	0.102	0.932	1.33	0.140	0.129	0.127
80	1.80	3.72	1.57	0.247	0.627	1.13	0.168	0.060	0.088
90	1.62	3.73	1.02	0.291	0.489	0.968	0.096	0.047	0.081
105	2.04	3.58	1.11	0.234	0.585	0.991	0.128	0.031	0.073
120	2.30	4.26	1.45	0.263	0.665	1.29	0.179	0.042	0.104
130	2.49	5.37	1.46	0.434	0.742	1.51	0.207	0.066	0.113
Error %	15.4	15.0	15.1	19.3	15.1	15.0	15.3	15.8	15.2

Table 3: Electron impact vibrational excitation DCSs from this work (in units of 10^{-18} cm^2/sr) and the average error of the DCSs in % units. The E_0 value is at the top left of each table.

E_L(eV)→	0.092		0.128		0.178		0.214		0.269	
E_0 (eV)?	ICS	Error	ICS	Error	ICS	Error	ICS	Error	ICS	Error
5	31.2	9.1	99.8	15.1	34.2	5.2	7.0	1.4	14.5	2.3
6	24.3	4.6	126	19	50.0	7.7	7.7	2.2	26.8	3.9
7.5	35.1	9.5	165	24	81.9	12.6	2.7	1.2	39.6	5.8
10	69.0	10.0	106	16	52.8	8.1	3.5	0.9	19.7	3.0
15	31.0	5.9	63.7	9.7	23.1	3.6	4.5	0.9	9.9	1.5

E_L(eV)→	0.391		0.514		0.58		0.751		Sum	
E_0 (eV)?	ICS	Error	ICS	Error	ICS	Error	ICS	Error	ICS	Error
5	86.2	12.94	11.5	1.72	4.96	0.80	6.96	1.07	296	44
6	98.4	14.49	15.9	2.51	6.47	0.98	8.97	1.34	365	55
7.5	106	15.91	16.0	2.53	7.70	1.36	10.1	1.6	465	70
10	70.4	10.59	8.4	1.32	2.95	0.56	5.53	0.86	338	51
15	18.3	2.70	2.4	0.39	0.91	0.17	1.50	0.24	155	23

Table 4: Electron impact vibrational excitation ICSs from this work and associated uncertainty (in units of 10^{-18} cm^2).

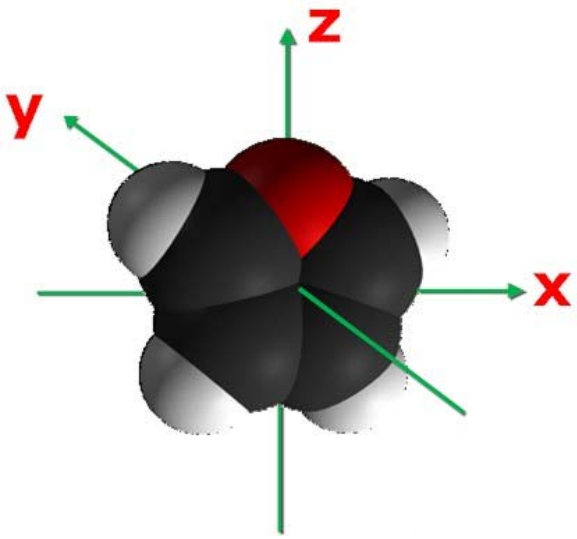

Figure 1 (Color online): Molecular space-filling model of furan. The symmetry axes refer to character table 1.

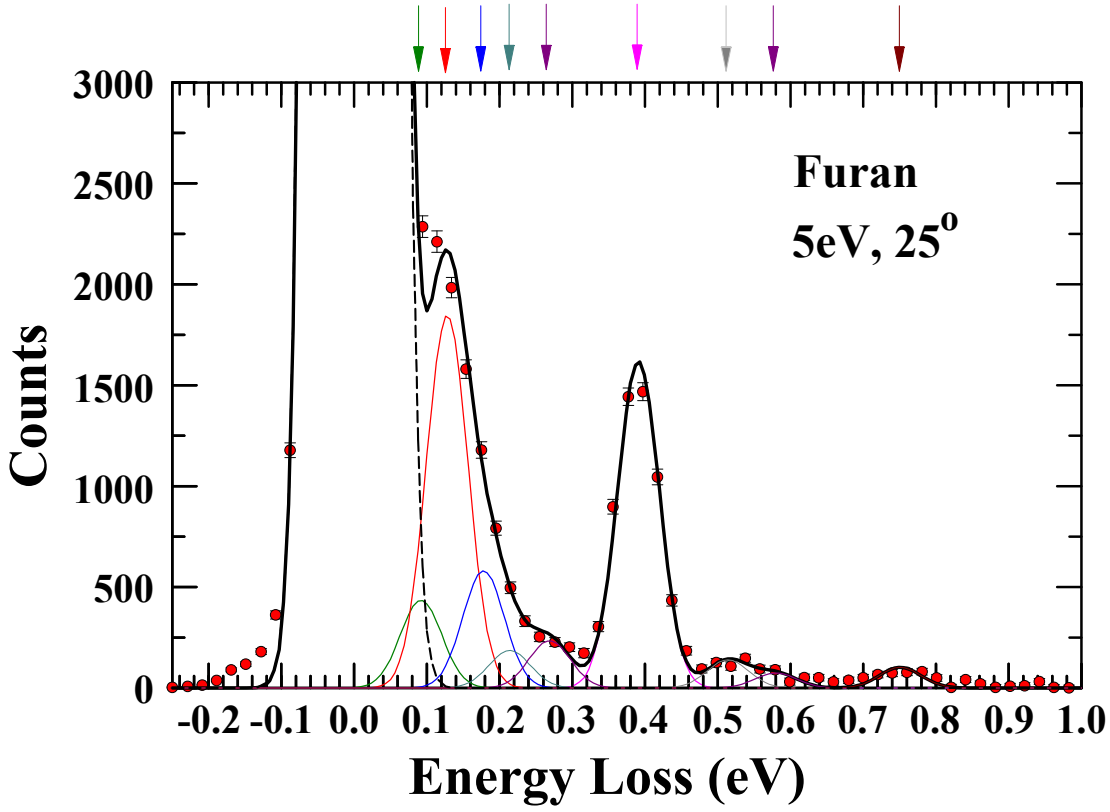

Figure 2 (Color online): Electron energy loss spectrum of furan taken at E_0=5eV and θ=25°. Legend: red dots with error bars are the experimental data; bold black line is the fit to the spectrum; colored full lines are the fits to individual features (located by their center by the arrows). The colored arrows show the positions of the resolved energy loss features at 0.092 , 0.128, 0.178, 0.214, 0.269, 0.391, 0.514, 0.580 and 0.751eV, respectively.

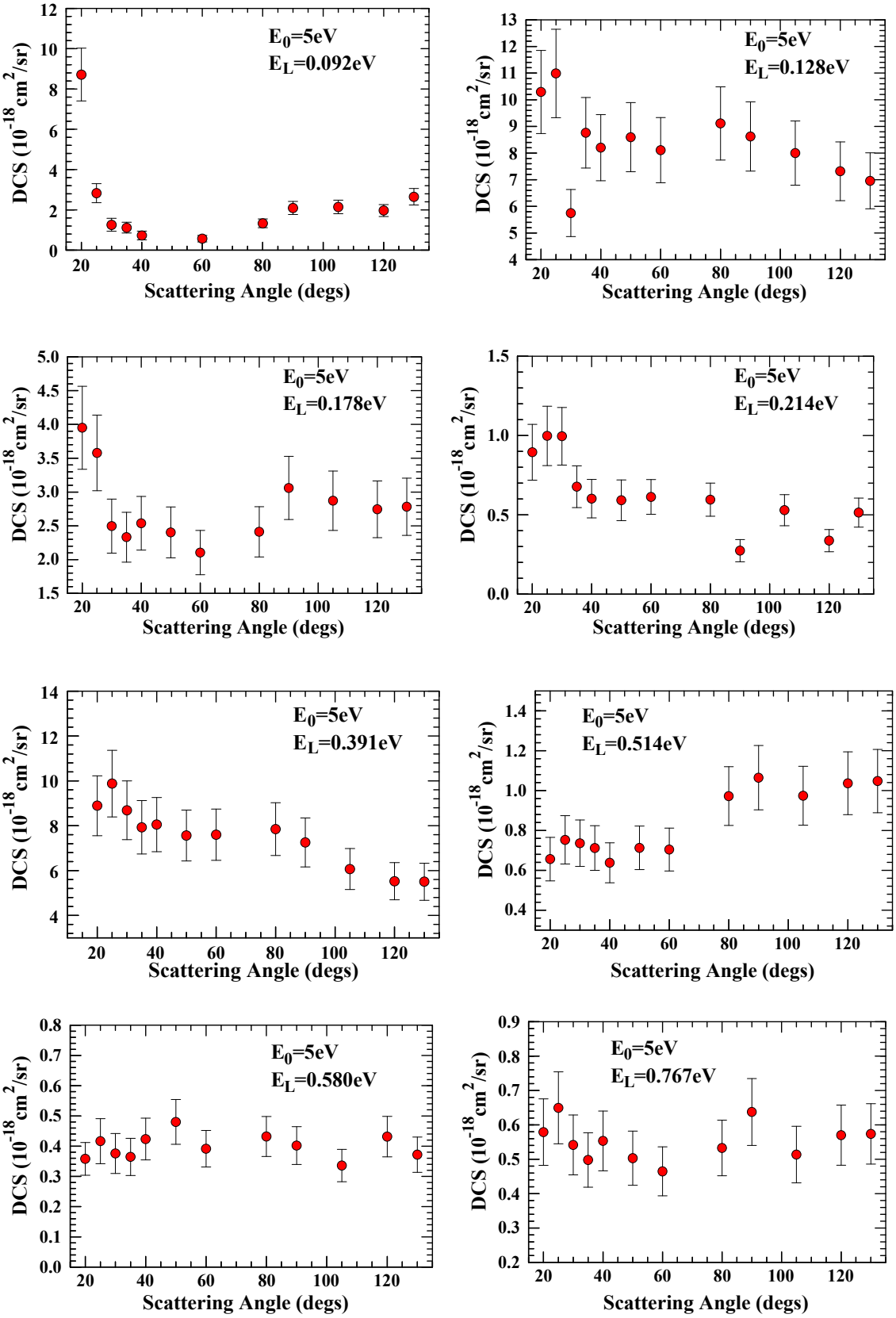

Figure 3a (Color online): Present differential cross-sections for the electron impact vibrational excitation features centered around the E_L values indicated for an E_0 value of 5eV.

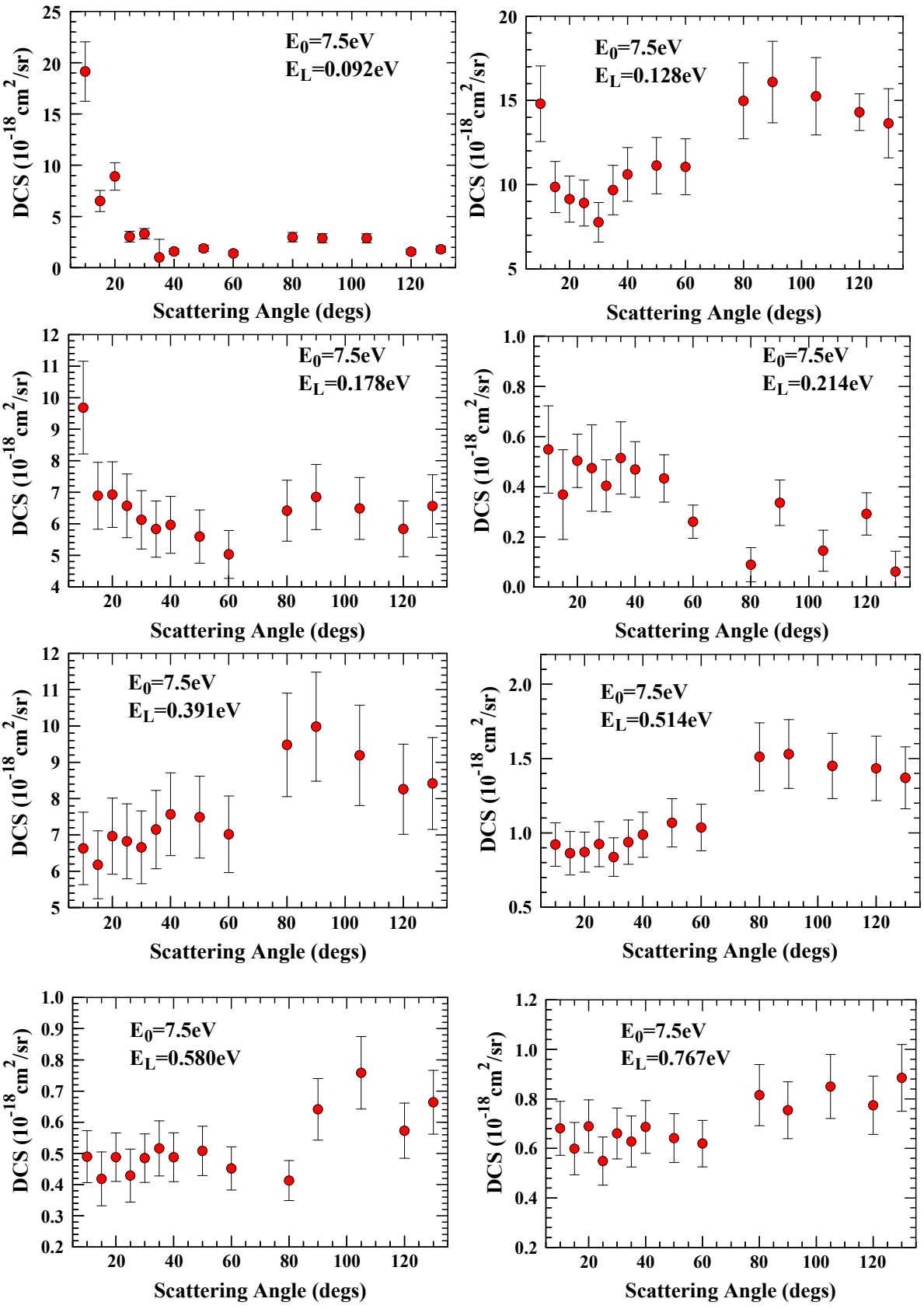

Figure 3b (Color online): Same as 3a, but for an E_0 value of 7.5eV.

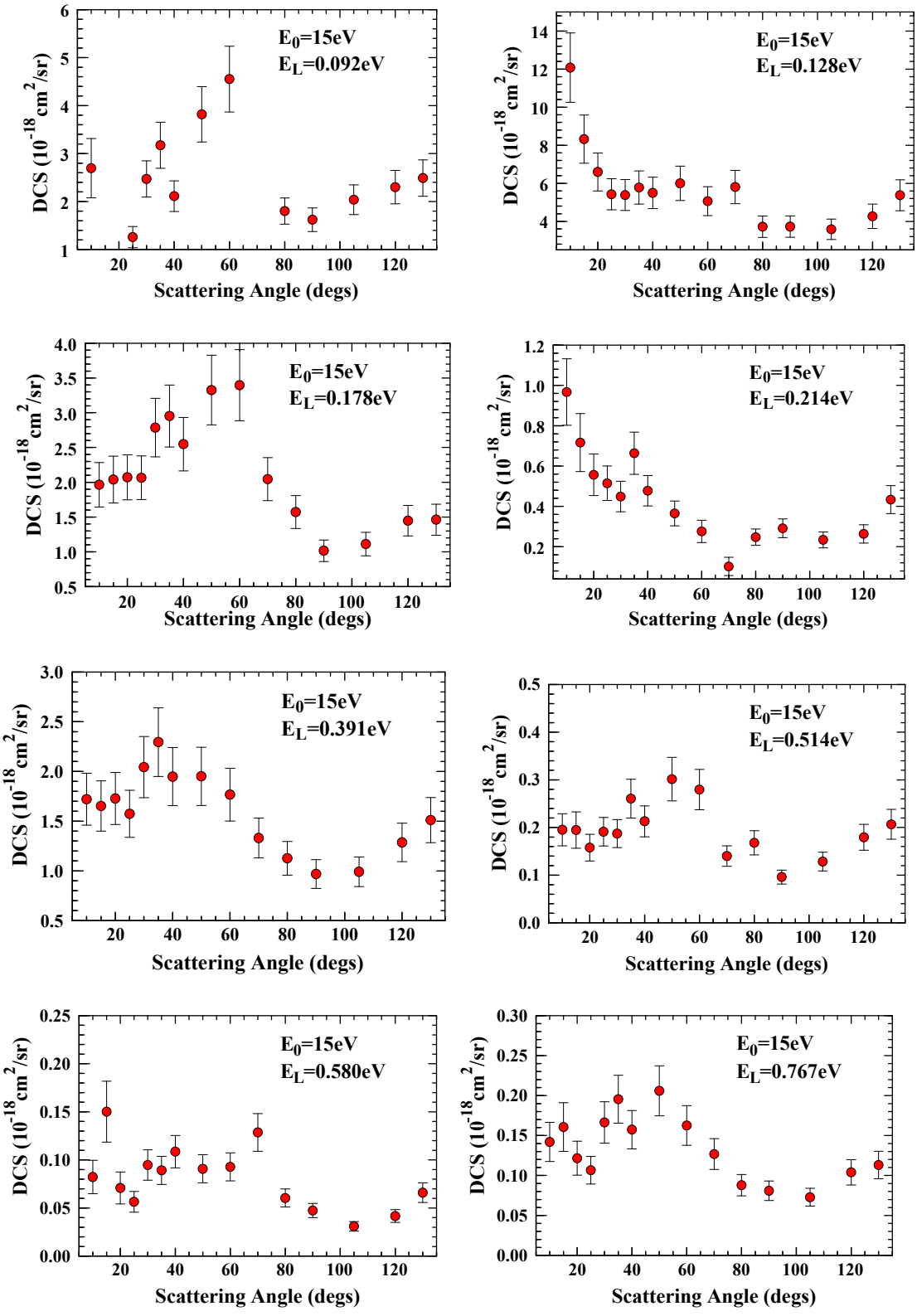

Figure 3c (Color online): Same as 3a, but for an E_0 value of 15eV.

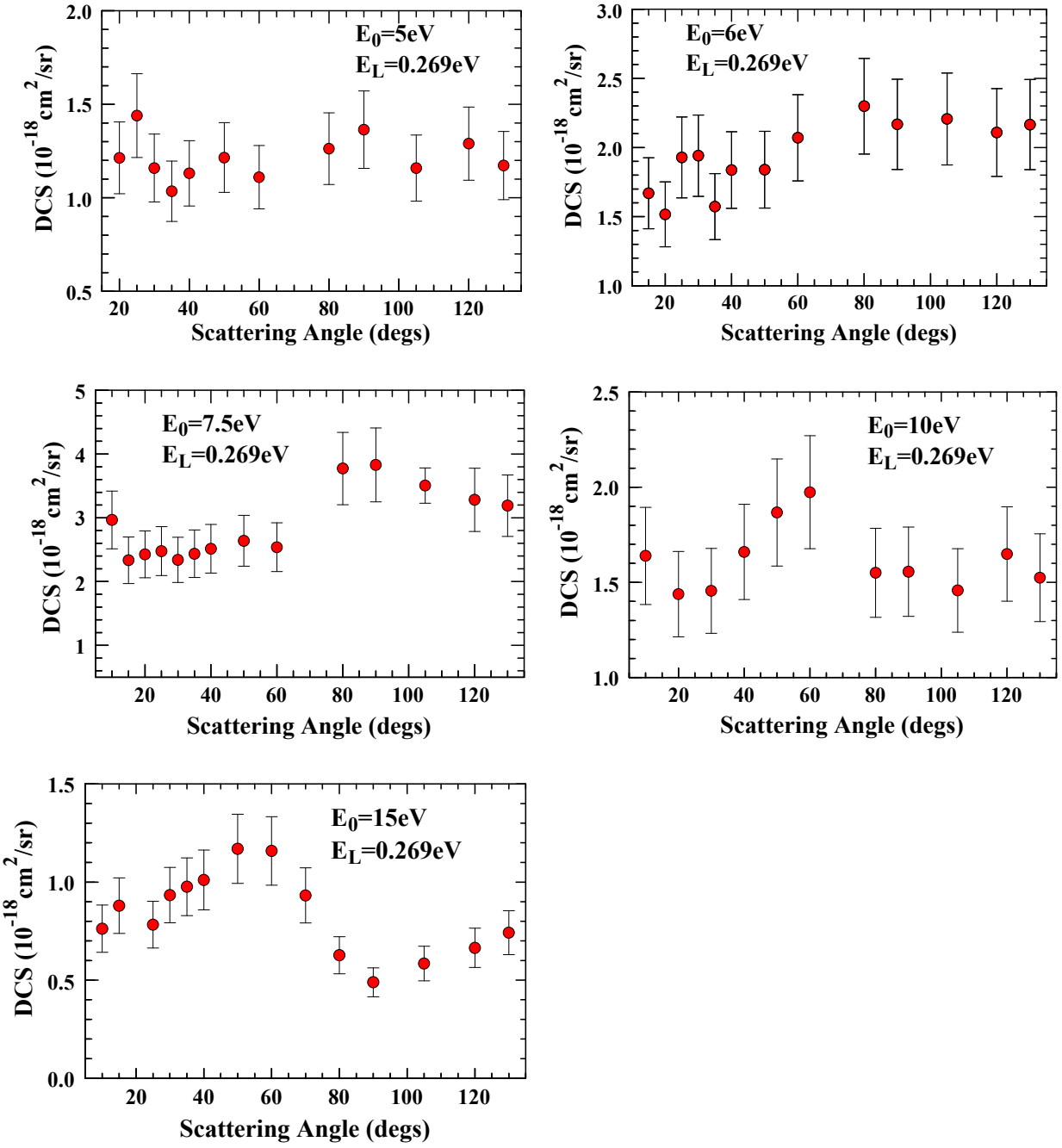

Figure 3d (Color online): Same as 3a, but for the E_L=0.269eV excitation of the (B_1, $\nu_7 + \nu_{19}$) vibrational mode at various E_0 values.

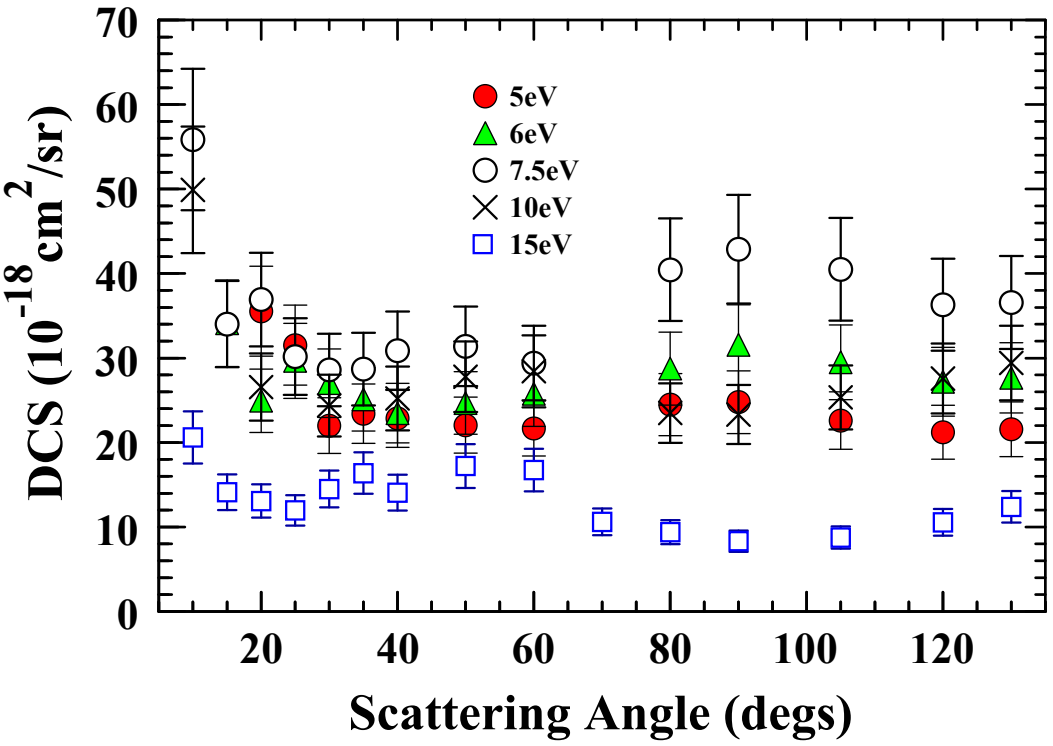

Figure 3e (Color online): Same as 3a, but for the sum of all vibrational excitation. Legend of E_0 values: ● 5eV, ▲ 6eV, ○ 7.5eV, ✕ 10eV and □ 15eV.

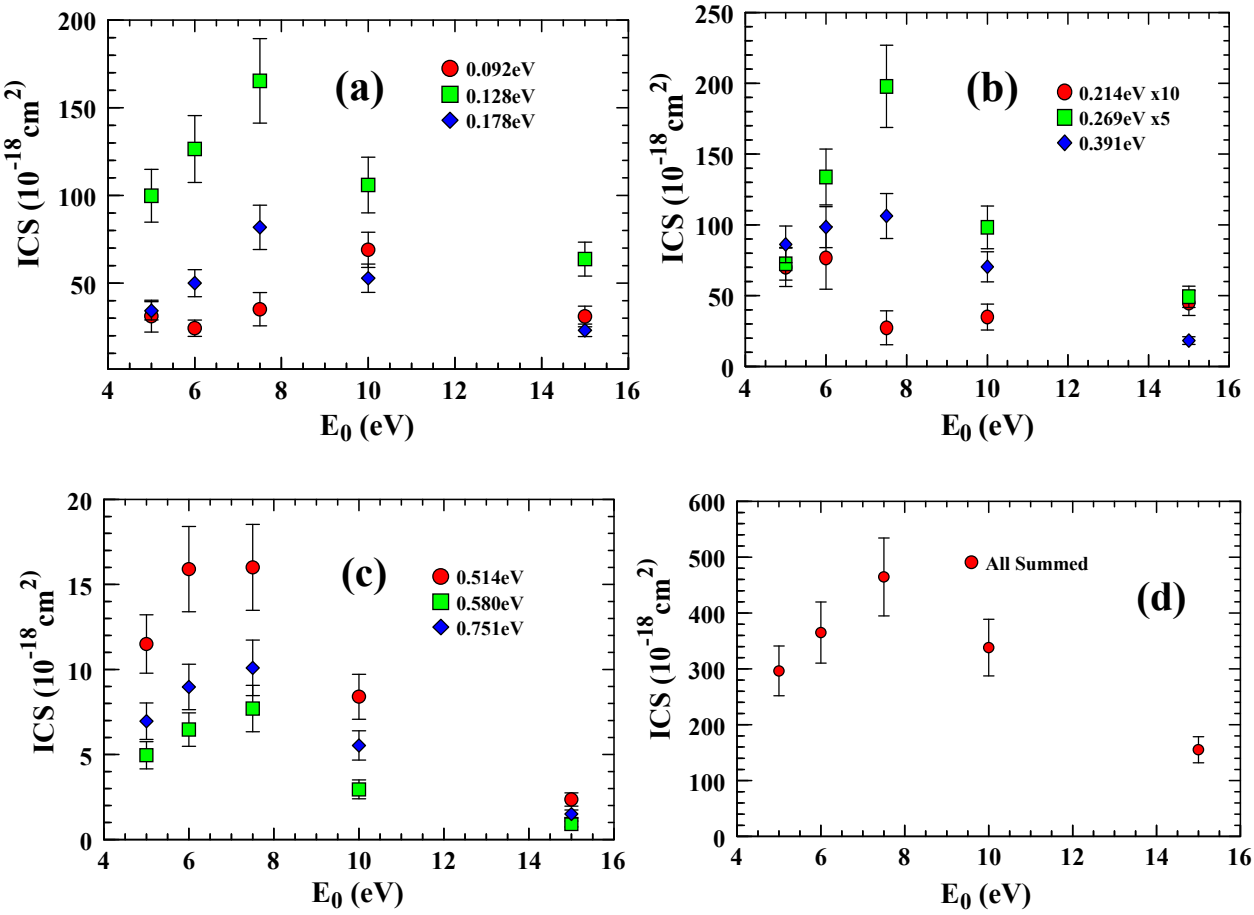

Figure 4a-d (Color online): Integral cross-sections for various E_L features (see legend) as a function of E_0. Note the multiplication factors for the 0.214eV and 0.269eV E_L features in 4(b).